



HHS Public Access

Author manuscript

Proceedings (IEEE Int Conf Bioinformatics Biomed). Author manuscript; available in PMC
2016 June 06.

Published in final edited form as:

Proceedings (IEEE Int Conf Bioinformatics Biomed). 2015 November ; 2015: 1253–1259. doi:10.1109/
BIBM.2015.7359860.

Comparison of an Atomic Model and Its Cryo-EM Image at the Central Axis of a Helix

Jing He¹, Stephanie Zeil¹, Hussam Hallak¹, Kele McKaig¹, Julio Kovacs², and Willy Wriggers²

¹Department of Computer Science, Old Dominion University, Norfolk, VA, 23529

²Department of Mechanical & Aerospace Engineering, Old Dominion University, Norfolk, VA, 23529

Abstract

Cryo-electron microscopy (cryo-EM) is an important biophysical technique that produces three-dimensional (3D) density maps at different resolutions. Because more and more models are being produced from cryo-EM density maps, validation of the models is becoming important. We propose a method for measuring local agreement between a model and the density map using the central axis of the helix. This method was tested using 19 helices from cryo-EM density maps between 5.5 Å and 7.2 Å resolution and 94 helices from simulated density maps. This method distinguished most of the well-fitting helices, although challenges exist for shorter helices.

Keywords

Validation; protein structure; secondary structure; image; fitting; cryo-electron microscopy

I. Introduction

Cryo-electron microscopy (cryo-EM) produces three-dimensional (3D) electron density maps of large protein complexes with a wide range of resolutions, from about 3 Å to more than 80 Å. As of September 2015, more than 3200 cryo-EM images have been deposited in the Electron Microscopy Data Bank (EMDB), and more than 890 atomic models have been derived from these density maps (<http://emdatbank.org/index.html>). The atomic models are linked to the Protein Data Bank (PDB). Some of the models are derived from cryo-EM density maps at about 3 Å resolution, and others are derived from medium resolutions (about 4–8 Å). The models are more likely to be correct for cryo-EM images with high resolutions, since more structural details are visible. The backbone of a protein structure is less resolved at medium resolutions, and deriving atomic structures is challenging. The current atomic models derived from cryo-EM images at medium resolutions are based on the fitting principle. This approach uses an atomic structure as a template to fit in the cryo-EM image. Rigid-body fitting and flexible fitting methods have been developed [2-4]. The *de novo* modeling approach does not rely on a known atomic structure [5-8]. This approach offers a

complementary approach when no suitable templates are found in the PDB. However, in spite of active development of the *de novo* approach [5, 6, 9], no mature tool for deriving atomic models for medium-resolution density maps is available.

The resolution of a density map is often used as a measurement of quality. However, resolution is a global measurement, and it is common to see local variations in quality for maps with similar resolutions and in different regions of the same density image (Figure 1). For example, in Figure 1, the upper helix has a strong cylinder characteristic, while the density of the lower helix does not resemble a cylinder in the same density map at the same density threshold. A similar problem may occur in a β -sheet, a turn or a loop. As more and more models are being deposited in the database, there is a need to develop a quantitative method for analyzing the fit locally at different regions.

Secondary structures such as helices and β -sheets are the most obvious structural components in medium-resolution images. Ideally, a secondary structure in an atomic model should appear as the corresponding secondary structure in the density image. The density features of a helix and a β -sheet have been well studied. In general, helices begin to become visible in cryo-EM maps at a resolution of about 10 Å, and long helices can be detected reliably at resolutions of 8 Å or better [10, 11]. β -sheets begin to be visible at a resolution of about 8 Å [10, 15]. Various computational methods have been developed to detect helices and β -sheets, including *SSEhunter*, *SSElearner*, *SSETracer* and *VolTrac* [10, 11, 16]. The assignment of secondary structure content relies on the detection of the cylindrical characteristic of a helix and the detection of the thin layer of density for a β -sheet. The success of these methods suggests that the density features of the secondary structures are visible in the image. Using *SSElearner*, about 75% of the helices can be detected in cryo-EM density maps at medium resolutions [11]. *SSETracer* has similar sensitivity as *SSElearner* [1]. In addition to helices, the location of β -strands can be predicted from a β -sheet density image [17, 18].

The current status of secondary structure detection is that major secondary structures such as long helices and large β -sheets can be detected in density maps at medium resolutions. The detection of smaller secondary structures is still challenging. The small secondary structures are easy to confuse among a short helix, a turn or a small two-stranded β -sheet. In order to improve the detection methods, a dataset of challenging cases on which current detection methods fail should be collected.

Validating a model is challenging, and various metrics may be utilized. Current atomic models derived from medium-resolution cryo-EM maps are obtained from fitting. Fitting an atomic model in a density map utilizes the entire density image. Although it is expected that a density image at medium resolution contains errors, it is not clear which features in the image are the most reliable. One may need to be careful using fine details of density variation in model validation. The work in this paper aimed at developing local measurement, the first step toward a more in-depth study of locally reliable features.

Since helices are the most visible density features in such density maps, in this paper, we investigate the possibility of quantifying models at helix regions using the cylindrical

characteristic of a helix. We compare the helix axis of an atomic model with that derived from the image. We show that the quantitative measurement of helix axes is a simple method for screening atomic models. This method can be used to identify models that fit well at the helix regions and models that are potentially challenging. Such collected challenging cases may provide insights for developing better methods for detecting secondary structures.

II. Methodology

A. The detection of helices in cryo-EM density maps

In a medium-resolution image, a helix appears as a cylinder. We applied *SSETracer*^[1] and enhanced the helix extension to detect the location of helices in a density map. *SSETracer* detects helices based on characterization of local density features. The local structure tensor, local thickness, continuity of the skeleton and density value are measured in *SSETracer*. The previous version of *SSETracer* was enhanced in the extension step. The newer version appears to detect longer helices than the previous version. A detected helix is represented by its central axis that is defined by a set of points.

B. Representation of a helix in an atomic model

A helix in an atomic model is reduced to the axial line of the helix in order to compare it with that in the image. Given the backbone position of a helix, the axis can be simply calculated by averaging the geometric positions of four consecutive Ca atoms on the helix. For a helix of length N , $N-3$ geometric centers are calculated. The resulting line contains a set of points that approximate the axis of the helix.

C. Distance between two axes of a helix

Given two axes of the helix, one detected in the image and one calculated from the atomic model, the distance between them is calculated. Each axis is represented as a set of points along the line. Note that the line is often not straight, particularly for long helices. In addition, note that the number of points on the two lines is often not the same. Let \mathcal{S} be the axis of a helix detected in a density map, and let \mathcal{S}' be the axis of the helix derived from the model. The two closest points on the axis form a line segment, and therefore, an axis can be thought of having a set of line segments. The distance between two sets of points was estimated as in (1). For each point $i, i=1, \dots, N$ on \mathcal{S} , we calculate $D_i^{\mathcal{S}\mathcal{S}'}$ that is the projection distance from i to the closest line segment of \mathcal{S}' . If the projection of i was outside the line segment, the distance between i and the closest end point of the line segment was used as the projection distance. Similarly, $D_j^{\mathcal{S}'\mathcal{S}}$ was calculated as the distance from each point $j, j=1, \dots, M$ of \mathcal{S}' to the closest line segment of \mathcal{S} .

$$D = \left(\sum_{i=1}^N D_i^{\mathcal{S}\mathcal{S}'} / N + \sum_{j=1}^M D_j^{\mathcal{S}'\mathcal{S}} / M \right) / 2 \quad (1)$$

The distance as calculated in (1) is a two-way distance. One way represents the distance from one line to the other, and the other represents the reverse. The larger the distance, the

larger the misalignment between the two lines. Note that D reflects a mixture of the lateral distance and the end-to-end distance between the two axes.

D. Detection of helix axes using VolTrac

VolTrac is a computational method for the detection of helices and filaments in a density map. This method combines a template-based search with a genetic algorithm to detect the initial positions of a helix. A bidirectional extension was used to define the axis of a helix [16, 21]. *VolTrac* uses a completely different search procedure from *SSETracer*, and therefore it offers an independent detection. *VolTrac* is embedded in Sculptor, a graphical interface for operations using atomic models and cryo-EM density maps.

III. Results

A. The datasets

Two datasets were used to compare the helices detected in the image with those derived from the corresponding atomic model. The first dataset contained nine proteins for which the atomic structures were downloaded from the PDB, and the corresponding 3D density maps were simulated using Chimera to 10 Å resolution [19]. The nine proteins of the simulated dataset included 92 helices. The second dataset contained four chains of proteins, for which the cryo-EM density maps were downloaded from the EMDB [20]. The cryo-EM dataset included 19 helices of four proteins. The cryo-EM density maps and their corresponding structures were EMD-1237-2GSY_A (7.2 Å), EMD-1733-3C91_H (6.8 Å), EMD-1780-3IZ5_J (5.5 Å) and EMD-5030-3FIN_R (6.4 Å). Three of the four cryo-EM density maps were aligned with their corresponding structures at download. For EMD-1237, manual alignment was performed first, and then the Fit-in-Map function of Chimera was used to optimize the fitting locally. The density maps of individual chains were extracted from the original density map of multiple chains using a mask of the chain derived from the PDB structure. *SSETracer* was applied to obtain the position of the helices from all the density maps in both datasets [1]. The distance between the two axial lines was calculated.

B. Tests using cryo-EM data

Figure 2 shows the axial lines derived from the helices in the atomic model and the lines from the image. In this case, the axes detected using *SSETracer* show various levels of agreement with those calculated from the model. The best-aligned cases are the first two helices, for which the two-way distances are only 1.06 Å and 0.92 Å, respectively (Table 1 rows 16–17). *SSETracer* detects helices based on the cylinder characteristic, skeleton, local thickness and density value. If a detected axis aligns well with that of a model helix, then the image of the model helix probably has good helix characteristics. Well-aligned axes provide more confidence in the model. The axis detected in image EMD-5030 does not align well with the axis calculated using the fourth helix of 3FIN chain R (Figure 2, row 4). The distance between the two axes is 3.96 Å for this case (Table 1, row 19). Close examination of this case shows that the density is more discontinuous at the high-density regions. Although there is a lateral distance between the two lines suggesting lateral misalignment, the main distance comes from the positioning of the helix. The model includes a helix-like region that appears to be similar to a helix in the image. Note that good alignment between

the two axes provides confidence in the model. However, bad alignment does not mean the model is wrong. Disagreement identifies a problem between the model and the image.

Of the 19 helices tested in the cryo-EM dataset, 14 had an axial distance of less than 2.5 Å, and only one helix (5030_R_72-81) had an axial distance of more than 2.5 Å. Four helices with 4, 5, 6 and 11 amino acids, respectively, were not detected by *SSETracer*. Helices shorter than two turns are often challenging to detect, but image quality is also an important factor. The longest helix in the dataset was 5030_R_57_38-57, which was 20 amino acids long (Figure 2). The helix had a small axial distance of 0.92 Å.

C. Tests using simulated density maps

The helix axes were compared using a larger simulated dataset. Nine protein structures were downloaded from the PDB and were used to simulate density maps at 10 Å resolution using Chimera. Because such simulated density maps represent noise-free density maps, they have much better quality than the cryo-EM density maps produced from the experiments. We simulated the density maps at lower resolution than the cryo-EM density maps in the first dataset in order to lower the quality to some extent. *SSETracer* detected 74 of the 94 helices with a less than 2 Å two-way distance. Thirty-five helices were detected within a 1 Å two-way distance from their model axes. Thirty-four of the accurately detected axes were 12 amino acids long or longer. For the helix with 17 amino acids (Figure 3, upper left panel), the two axes appear to align very well. In this case, the two-way distance is only 0.67 Å. The results suggest that the axes detected in simulated density maps are accurate for long helices. Short helices remain challenging; 14 of the 94 helices were not detected.

Only four of the 94 helices had an axial distance longer than 2.0 Å. One case is shown in row 3 of Figure 3. The PDB structure has two helices (1UNF 36-44 and 46-59) that are in a similar direction but split by one amino acid. Since the two helices are in the same direction, they appear as one long helix instead of two shorter helices. Such split cases show large two-way distances, 2.98 Å in this case (Table 2, row 19). Another case with a large two-way distance is shown for 1UNF HLX 10 and 11 (Figure 3, middle right panel). Two helices with four and six amino acids, respectively, are consecutive in sequence but have slightly different directions. As the image does not resolve such situations clearly, it shows a connected short helix. Even after we generated an axis using the two shorter consecutive helices, the two axes (purple and yellow) had a large misalignment. In this case, the two-way distance is 2.48 Å.

D. Helix axes detected using two alternative methods

We applied *VolTrac* to four cryo-EM density maps. The axes detected by *VolTrac* were mostly similar to those detected by *SSETracer*, particularly for long helices. As an example, for EMD-1733, the two sets of axes (red and green lines in Figure 4) aligned well for all five helices. Both tools detected similar helix axes, which suggest that the density features of the helices are strong in this map. Three of the four helices in EMD-5030-PDB-3FIN_R (Figure 4 A and B) align well, although the length of H2 differs. The two methods do not agree well on helix H4. In fact, this helix was ranked the fifth highest by *VolTrac*, suggesting that the density at this region is not as characteristic of a cylinder as that of the other three helices.

Also, the H4 axis detected by *SSETracer* does not align well with that of the atomic structure. The disagreement between two methods suggests that the cryo-EM density in that region needs to be studied further.

In a preliminary sensitivity / specificity analysis, we found that *VolTrac* is more sensitive but less specific than *SSETracer*. The observed sensitivity of *VolTrac* was 91.5%, but only 64.4% for *SSETracer* in the case of EMD-5030. The specificity of *SSETracer* was 94.8%, but 84.5% for *VolTrac* in this case. The specificity was computed by counting the number of C α atoms in the structure that were correctly detected. A correctly detected C α atom is one that has a point on the detected axis line within 2.75 Å distance. Although a more systematic analysis will be carried out in the future, the current four cases suggest that *VolTrac* is more sensitive and *SSETracer* is more specific.

Each method has advantages and disadvantages, and the methods could be combined for more accurate detection of helices. One disadvantage of *VolTrac* is the run-time needed to perform an exhaustive template-based search using a genetic algorithm. *SSETracer* is much faster in finding initial candidate locations of helices since the search is template-free. This could be combined with the bidirectional expansion of *VolTrac* that provides smoother and longer helix axes (Fig. 4 B) compared to *SSETracer*.

IV. Summary

As more and more atomic models are being produced from cryo-EM density maps, validation of the models is becoming important. The models are generally expected to be energetically stable and to agree well with the corresponding cryo-EM density maps. Correlation is widely used for fitting of atomic models. However, it is not easy to consider local properties in such a global measure. In addition, until a systematic analysis is performed, it is not clear which regions in a medium-resolution image are most reliable. Since helices are the dominant secondary structure feature, we investigated the possibility of using helices as a landmark to evaluate the quality of an atomic interpretation in the helix region. Although it has long been established that helices are detectable in density maps with better than 10 Å resolution, it has not been clear if the detected helix axes are accurate enough to quantify the local difference between an atomic model and its image. For noise-free density maps, our test of 94 helices showed that 74 helices were detected to within 2 Å accuracy. Helices longer than 12 amino acids are more suitable for the assessment of cryo-EM images and atomic models. More accurate handling of the ends of an axis will be the focus of future work. Combining advantages of multiple methods, such as *SSETracer* and *VolTrac*, may also enhance the detection accuracy.

ACKNOWLEDGMENT

The work in this paper was partially supported by NSF DBI-1356621, NIH R01-GM062968, and the Honors College of Old Dominion University.

REFERENCES

- [1]. SI, D.; HE, J. BETA-SHEET DETECTION AND REPRESENTATION FROM MEDIUM RESOLUTION CRYO-EM DENSITY MAPS; BCB'13: PROCEEDINGS OF ACM

CONFERENCE ON BIOINFORMATICS, COMPUTATIONAL BIOLOGY AND BIOMEDICAL INFORMATICS; WASHINGTON, D.C.. 2013. p. 764-70.

- [2]. ROSSMANN MG. FITTING ATOMIC MODELS INTO ELECTRON-MICROSCOPY MAPS. ACTA CRYSTALLOGR D BIOL CRYSTALLOGR. Oct.2000 56:1341–9. [PubMed: 10998631]
- [3]. SCHRÖDER GF, BRUNGER AT, LEVITT M. COMBINING EFFICIENT CONFORMATIONAL SAMPLING WITH A DEFORMABLE ELASTIC NETWORK MODEL FACILITATES STRUCTURE REFINEMENT AT LOW RESOLUTION. STRUCTURE (LONDON, ENGLAND : 1993). 2007; 15:1630–1641.
- [4]. WRIGGERS W, BIRMANNS S. USING SITUS FOR FLEXIBLE AND RIGID-BODY FITTING OF MULTIREOLUTION SINGLE-MOLECULE DATA. J STRUCT BIOL. Feb-Mar;2001 133:193–202. [PubMed: 11472090]
- [5]. BAKER ML, ABEYSINGHE SS, SCHUH S, COLEMAN RA, ABRAMS A, MARSH MP, et al. MODELING PROTEIN STRUCTURE AT NEAR ATOMIC RESOLUTIONS WITH GORGON. JOURNAL OF STRUCTURAL BIOLOGY. 2011; 174:360–373. [PubMed: 21296162]
- [6]. AL NASR K, RANJAN D, ZUBAIR M, CHEN L, HE J. SOVLING THE SECONDARY STRUCTURE MATCHING PROBLEM IN CRYO-EM DE NOVO MODELING USING A CONSTRAINED K-SHORTEST PATH GRAPH ALGORITHM. IEEE/ACM TRANS COMPUT BIOL BIOINFORM. 2014; 11:419–29. [PubMed: 26355788]
- [7]. AL NASR K, SUN W, HE J. STRUCTURE PREDICTION FOR THE HELICAL SKELETONS DETECTED FROM THE LOW RESOLUTION PROTEIN DENSITY MAP. BMC BIOINFORMATICS. 11(SUPPL 1):S44. [PubMed: 20122218]
- [8]. LINDERT S, STARITZBICHLER R, WÖTZEL N, KARAKAS M, STEWART PL, MEILER J. EM-FOLD: DE NOVO FOLDING OF ALPHA-HELICAL PROTEINS GUIDED BY INTERMEDIATE-RESOLUTION ELECTRON MICROSCOPY DENSITY MAPS. STRUCTURE. Jul 15.2009 17:990–1003. [PubMed: 19604479]
- [9]. LINDERT S, ALEXANDER N, WOTZEL N, KARAKA M, STEWART PL, MEILER J. EM-FOLD: DE NOVO ATOMIC-DETAIL PROTEIN STRUCTURE DETERMINATION FROM MEDIUM-RESOLUTION DENSITY MAPS. STRUCTURE (LONDON, ENGLAND: 1993). 2012; 20:464–478.
- [10]. BAKER ML, JU T, CHIU W. IDENTIFICATION OF SECONDARY STRUCTURE ELEMENTS IN INTERMEDIATE-RESOLUTION DENSITY MAPS. STRUCTURE. Jan.2007 15:7–19. [PubMed: 17223528]
- [11]. SI D, JI S, NASR KA, HE J. A MACHINE LEARNING APPROACH FOR THE IDENTIFICATION OF PROTEIN SECONDARY STRUCTURE ELEMENTS FROM ELECTRON CRYO-MICROSCOPY DENSITY MAPS. BIOPOLYMERS. Sep.2012 97:698–708. [PubMed: 22696406]
- [12]. JIANG W, BAKER ML, LUDTKE SJ, CHIU W. BRIDGING THE INFORMATION GAP: COMPUTATIONAL TOOLS FOR INTERMEDIATE RESOLUTION STRUCTURE INTERPRETATION. J MOL BIOL. May.2001 308:1033–44. [PubMed: 11352589]
- [13]. DAL PALU A, HE J, PONTELLI E, LU Y. IDENTIFICATION OF ALPHA-HELICES FROM LOW RESOLUTION PROTEIN DENSITY MAPS. PROCEEDING OF COMPUTATIONAL SYSTEMS BIOINFORMATICS CONFERENCE(CSB). 2006:89–98.
- [14]. KONG Y, ZHANG X, BAKER TS, MA J. A STRUCTURAL-INFORMATICS APPROACH FOR TRACING BETA-SHEETS: BUILDING PSEUDO-C(ALPHA) TRACES FOR BETA-STRANDS IN INTERMEDIATE-RESOLUTION DENSITY MAPS. J MOL BIOL. May 21.2004 339:117–30. [PubMed: 15123425]
- [15]. ZEYUN Y, BAJAJ C. COMPUTATIONAL APPROACHES FOR AUTOMATIC STRUCTURAL ANALYSIS OF LARGE BIOMOLECULAR COMPLEXES. COMPUTATIONAL BIOLOGY AND BIOINFORMATICS, IEEE/ACM TRANSACTIONS ON. 2008; 5:568–582.
- [16]. RUSU M, WRIGGERS W. EVOLUTIONARY BIDIRECTIONAL EXPANSION FOR THE TRACING OF ALPHA HELICES IN CRYO-ELECTRON MICROSCOPY RECONSTRUCTIONS. J STRUCT BIOL. Feb.2012 177:410–9. [PubMed: 22155667]

- [17]. SI D, HE J. TRACING BETA-STRANDS USING STRANDTWISTER FROM CRYO-EM DENSITY MAPS AT MEDIUM RESOLUTIONS. STRUCTURE. 2014; 22(11):1665–76. 22. [PubMed: 25308866]
- [18]. SI, D.; HE, J. PROCEEDING OF EMBC. CHICAGO: 2014. COMBINING IMAGE PROCESSING ANND MODELING TO GENERATE TRACES OF BETA-STRANDS FROM CRYO-EM DENSITY IMAGES OF BETA-BARRELS.
- [19]. PETERSEN E, GODDARD T, HUANG C, COUCH G, GREENBLATT D, MENG E, et al. UCSF CHIMERA--A VISUALIZATION SYSTEM FOR EXPLORATORY RESEARCH AND ANALYSIS. J COMPUT CHEM. 2004; 25:1605–12. [PubMed: 15264254]
- [20]. LAWSON CL, BAKER ML, BEST C, BI C, DOUGHERTY M, FENG P, et al. EMDATABANK.ORG: UNIFIED DATA RESOURCE FOR CRYOEM. NUCLEIC ACIDS RES. Jan.2011 39:D456–64. [PubMed: 20935055]
- [21]. RUSU M, STAROSOLSKI Z, WAHLE M, RIGORT A, WRIGGERS W. AUTOMATED TRACING OF FILAMENTS IN 3D ELECTRON TOMOGRAPHY RECONSTRUCTIONS USING SCULPTOR AND SITUS. J STRUCT BIOL. May.2012 178:121–8. [PubMed: 22433493]

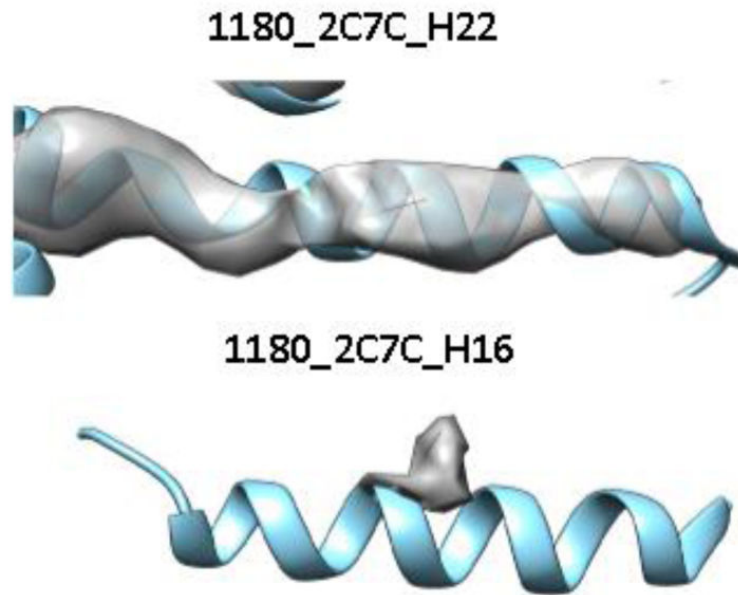


Figure 1.
Local density variation at helix regions. The EMD ID and the PDB ID are labeled for the two cases.

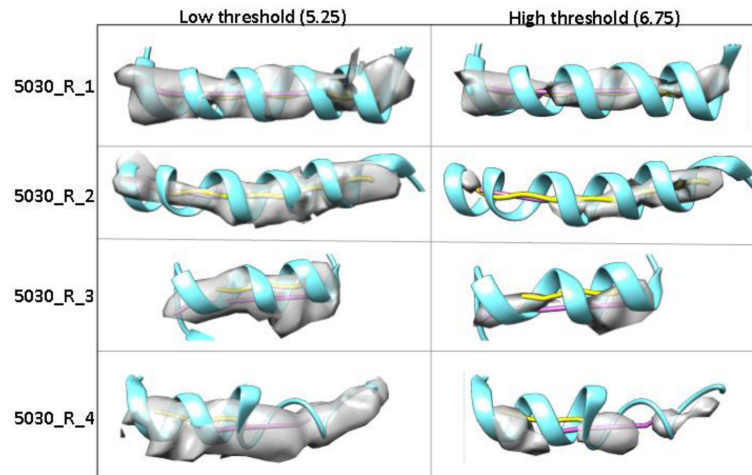


Figure 2. Comparison of a helix model with its cryo-EM density for EMD-5030/PDB-3FIN R chain. The axis (yellow line) derived from the atomic model, the axis (purple line) detected from the image are superimposed with the atomic model (ribbon) and the image (gray).

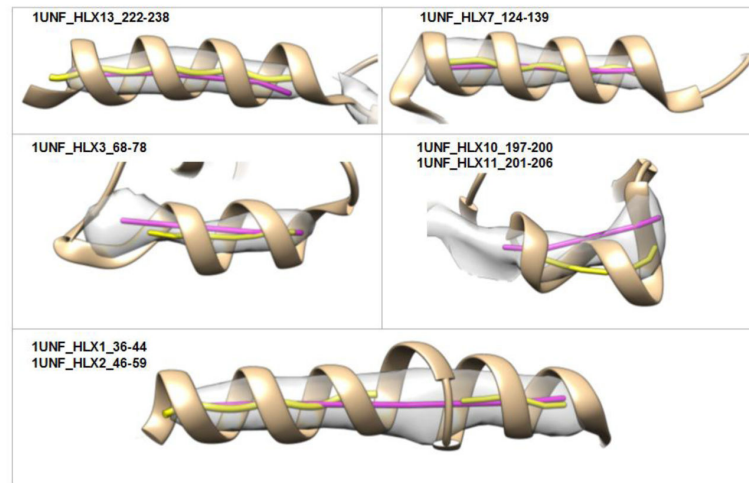


Figure 3.

Comparison of helix axes for a simulated image. The PDB structure 1UNF was used to generate a density image using Chimera. The axis (yellow line) calculated from the atomic model and the axis (purple line) detected from the image using *SSETracer* are superimposed with the atomic model (ribbon) and the image (gray).

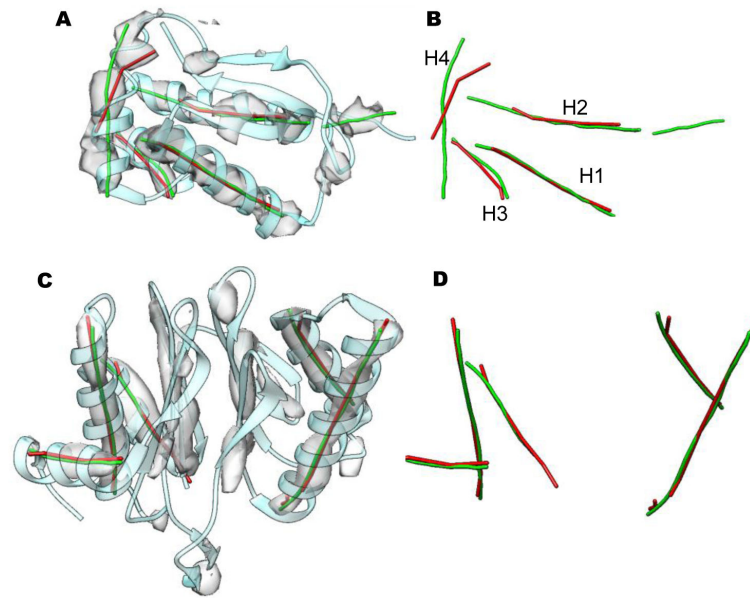


Figure 4. Axes of helices detected from the cryo-EM image using *SSETracer* and *VolTrac*. Helix axes detected from cryo-EM density map EMD-5030 in (A) and (B) and EMD-1733 in (C) and (D) using *SSETracer* [1] (red) and *VolTrac* (green) are superimposed with the image (gray) and the corresponding atomic model PDB-3FIN_R in (A) and PDB-3C91_H in (C) (ribbon). The label of helices in (B) correspond to those in Fig. 2.

Table 1

Helix axial distance between an atomic model and its cryo-EM image.

Index	Helix ID ^a	Distance (Å) ^b
1	1237_A_1_12-24	2.37
2	1237_A_2_91-94	N/A
3	1237_A_3_132-136	N/A
4	1237_A_4_142-147	N/A
5	1237_A_6_297-301	2.37
6	1237_A_7_378-382	1.72
7	1237_A_8_393-409	1.15
8	1237_A_9_416-426	1.20
9	1733_H_1_48-71	1.00
10	1733_H_2_75-90	0.93
11	1733_H_3_130-142	2.38
12	1733_H_4_147-166	1.23
13	1733_H_5_188-200	1.44
14	1780_J_1_39-58	1.29
15	1780_J_2_105-115	N/A
16	5030_R_56_13-31	1.16
17	5030_R_57_38-57	0.92
18	5030_R_58_59-68	2.36
19	5030_R_59_72-81	3.96

^aEMDB ID, the chain ID in the PDB file, the helix ID and the first and last amino acid indices for the helix.

^bThe two-way distance between the axis of a detected helix and the corresponding axis in the atomic structure. N/A means no detection in the cryo-EM image.

Table 2

Helix axial distance between an atomic model and its simulated image.

Index	Helix ID ^a	Distance (Å) ^b
1	1FLP_1_4-19	1.13
2	1FLP_2_21-35	1.11
3	1FLP_3_37-41	3.21
4	1FLP_4_59-76	1.23
5	1FLP_5_82-97	1.12
6	1FLP_6_103-116	1.75
7	1FLP_7_124-138	1.68
8	1HG5_1_19-30	1.28
9	1HG5_2_38-50	1.50
10	1HG5_3_55-67	0.89
11	1HG5_4_71-89	1.19
12	1HG5_5_90-100	1.56
13	1HG5_6_114-142	0.57
14	1HG5_7_160-180	2.40
15	1HG5_8_184-188	N/A
16	1HG5_9_190-222	0.88
17	1HG5_10_228-258	0.64
18	1HG5_11_260-264	N/A
19	1UNF_1_36-44	2.98
20	1UNF_2_46-59	1.01
21	1UNF_3_68-78	1.87
22	1UNF_5_85-101	N/A
23	1UNF_6_111-123	0.62
24	1UNF_7_124-139	N/A
25	1UNF_8_152-155	N/A
26	1UNF_9_181-185	N/A
27	1UNF_10_197-200	2.48 ^c
28	1UNF_11_201-206	2.48 ^c
29	1UNF_12_208-220	1.83
30	1UNF_13_222-238	0.67
31	2OVJ_1_350-355	N/A
32	2OVJ_2_363-377	0.96
33	2OVJ_3_389-402	0.76
34	2OVJ_4_408-412	N/A
35	2OVJ_5_414-428	1.26
36	2OVJ_6_438-448	N/A

Index	Helix ID ^a	Distance (Å) ^b
37	2OVJ_7_450-464	1.27
38	2OVJ_8_466-486	1.53
39	2OVJ_9_492-505	0.82
40	2OVJ_10_513-534	0.71
41	2OVJ_11_535-541	0.84
42	3E46_1_2-19	1.10 ^c
43	3E46_2_19-24	1.10 ^c
44	3E46_3_93-97	N/A
45	3E46_4_105-119	0.66
46	3E46_5_127-137	1.95
47	3E46_6_137-154	1.72
48	3E46_7_159-172	0.58
49	3E46_8_175-186	0.93
50	3E46_9_189-200	0.62
51	1LWB_1_4-12	1.56
52	1LWB_2_16-29	0.61
53	1LWB_3_30-37	N/A
54	1LWB_4_57-75	0.74
55	1LWB_5_76-97	0.65
56	1LWB_6_100-120	1.07
57	1NG6_1_2-17	0.54
58	1NG6_2_19-40	0.46
59	1NG6_3_46-72	0.44
60	1NG6_4_73-88	1.12
61	1NG6_6_96-111	0.70
62	1NG6_8_118-131	1.11
63	1NG6_9_135-147	0.59
64	3IEE_1_32-57	0.65
65	3IEE_2_58-73	1.18
66	3IEE_3_90-95	1.66
67	3IEE_4_102-136	1.34
68	3IEE_5_138-179	0.77
69	3IEE_6_184-206	1.88
70	3IEE_7_212-232	1.01
71	3IEE_8_239-264	1.35
72	3IEE_9_270-285	1.95
73	1HZ4_1_4-25	0.56
74	1HZ4_2_27-41	N/A

Index	Helix ID ^a	Distance (Å) ^b
75	1HZ4_3_46-65	0.80
76	1HZ4_4_66-84	0.58
77	1HZ4_5_86-104	1.29
78	1HZ4_6_106-124	0.59
79	1HZ4_7_130-146	N/A
80	1HZ4_8_148-163	0.79
81	1HZ4_9_167-170	1.01 ^c
82	1HZ4_10_171-186	1.01 ^c
83	1HZ4_11_187-203	0.60
84	1HZ4_12_208-226	0.91
85	1HZ4_13_228-239	N/A
86	1HZ4_15_250-264	N/A
87	1HZ4_16_266-284	0.58
88	1HZ4_17_286-305	0.80
89	1HZ4_18_306-325	0.55
90	1HZ4_19_327-332	N/A
91	1HZ4_20_333-347	0.88
92	1HZ4_21_351-366	N/A

^aThe PDB ID, the helix ID and the first and last amino acid indices for the helix.

^bThe two-way distance between the axis of a detected helix and the corresponding axis in the atomic structure. N/A means no detection in the cryo-EM image.

^cDistance value calculation based on a combination of this helix and an adjacent helix.